Progress In Electromagnetics Research M, Vol. 104, 111–122, 2021

Torque Ripple Online Optimization of Switched Reluctance Motor Based on Torque Slope Characteristics

Hanbing Yang[1], Aide Xu[2, *], Jianping Cheng[1], and Jinghao Sun[1]

Abstract—In this paper, a direct instantaneous torque control (DITC) optimization scheme based on adaptive dynamic hysteresis (ADH) strategy is proposed for switched reluctance motor (SRM) drive system. This method can further improve the torque tracking accuracy, reduce torque ripple, and enhance the smoothness between phases transition of SRM. According to the torque generation characteristics and hysteresis rule of DITC, the traditional hysteresis rule is modified, and the sampled discrete torque slope data are compensated online. Taking the slope curve after compensation as the standard, the upper and lower limits of the hysteresis controller are assigned to achieve the control effect of hysteresis dynamic regulation. The effectiveness of the method is verified by simulation under different operating conditions.

1. INTRODUCTION

Switched reluctance motor (SRM) has drawn growing attention in the industry in recent decades due to its simple structure, low cost, high reliability, and wide speed range [1–3]. However, due to its unique doubly salient structure and discrete mechanical conduction mechanism, its electromechanical conversion mode is highly nonlinear, and its control mode is significantly different from the traditional motor [4–6]. Large torque ripple is a major problem caused by the inherent characteristics, which also limits the application of SRM. In order to reduce the torque ripple of SRM, many advanced torque control strategies have been proposed in recent years.

Generally, torque control is divided into two categories: indirect control and direct control. Indirect torque control mainly depends on circuit profiling and torque sharing function (TSF). References [7, 8] optimize the current profiling to reduce the torque ripple. The former improves the tracking accuracy of the current profiling, and the latter calculates the optimal value of the current profiling. In [9], considering the influence of magnetic saturation and the minimum power loss in commutation region, the optimal TSF is selected by finding the tangent between the constant curve and the minimum radius circle on the commutation current plane. In [10], a novel and simple nonlinear logic TSF is proposed by using nonlinear TSF to control the current of adjacent two phases. The indirect torque control algorithm has strict requirements on the reverse torque model of the motor. Due to the complex electromagnetic relationship and high saturation nonlinearity of SRM, the structure of the reverse distance model is complex, and the amount of calculation of relevant control systems will also be seriously increased [11].

The direct control strategy can be subdivided into direct torque control (DTC) and direct instantaneous torque control (DITC). In essence, DTC and DITC belong to bang-bang hysteresis control strategy, which has the advantages of simple structure and good transient performance [12, 13]. DTC strategy optimization is mainly based on sector partition. References [14] and [15] improve the torque

Received 25 July 2021, Accepted 17 August 2021, Scheduled 26 August 2021

* Corresponding author: Aide Xu (aidexu@dlmu.edu.cn).

[1] College of Electrical Engineering of Ships, Dalian Maritime University, Dalian 116026, China. [2] College of Information and Science Technology, Dalian Maritime University, Dalian 116026, China.

by adjusting the sector partition of DTC and selecting appropriate voltage vectors to reduce the torque-current ratio in order to eliminate the influence of negative torque. In addition, the paper [14] adds power loss module to evaluate the drive system efficiency, and the optimized DTC method has a good performance in terms of efficiency and torque ripple.

Compared with DTC strategy, DITC strategy abandons the hysteresis of flux linkage and takes the instantaneous torque as the controlled object directly. Therefore, in terms of torque ripple suppression, DITC is superior to other traditional control algorithms. In recent years, related DITC optimization algorithms have been proposed gradually. In [16], mutual coupling effect is incorporated into DITC mechanical model to reduce the influence of winding distribution on output torque and harmonic. Reference [17] changes the connection mode of power converter to replace each phase branch current sensor and topologically improves DITC strategy to reduce costs and make the structure more compact. Reference [18] uses PWM instead of hysteresis controller in traditional DITC, analyses the torque pulsation during commutation, and puts forward the corresponding compensation method. Reference [19] optimizes the DTC torque hysteresis control scheme under different operation modes according to the torque-current ratio. Reference [20] realizes online adjustment of conduction angle and cutoff angle without using complex algorithm, which improves the system efficiency of DITC control strategy.

All the DITC optimization algorithms mentioned above improve the torque performance of SRM, and all of them are based on hysteresis control strategy optimization. However, there is still a tolerance problem which cannot be ignored in the hysteresis control and will directly lead to the increase of torque ripple. When the hysteresis width is too large or too small, the system will have over-modulation or under-modulation problems. When the sampling time is small enough, the SRM drive system can be considered as a discrete system. Due to the highly saturated and nonlinear electromagnetic relationship of SRM, the hysteresis threshold will change under different load conditions, so it is necessary to adjust the hysteresis threshold width adaptively according to the torque.

In this paper, a novel DITC adaptive dynamic hysteresis (ADH) optimization scheme for an SRM drive system is proposed,and the effect of hysteresis on torque ripple is fully considered. Firstly, the reason of the torque pulsation is analyzed in detail. And the concept of torque slope is put forward. Then the ADH module is added to improve the traditional DITC torque hysteresis part. Finally, the ADH optimized DITC based on the new hysteresis scheme aims to improve the efficiency of the system to control the torque. By analyzing the relationship between the hysteresis controller and the SRM discrete system, the control precision of the torque is improved. The optimization method can effectively reduce the torque pulsation and improve the smooth transition between phases.

2. ANALYSIS OF TRADITIONAL DITC STRATEGY

2.1. DITC

DITC is an optimal control strategy which takes the torque as the optimization objective, the system schematic diagram is shown in Fig. 1. The drive circuit of the DITC system adopts an asymmetric half bridge (AHB) circuit, and the current and angular position are used as feedback values to determine the reference torque by look-up table. According to the hysteresis scheme, the three states of the AHB in single-phase and commutation-phase are configured to achieve direct control of the instantaneous torque.

Figure 2 shows the three states of three phase AHB circuit driving SRM. Both upper and lower arms switched on is called magnetized state ($S = 1$). The situation in which only one of the upper and lower bridge arms conducts is called freewheeling state ($S = 0$). Simultaneous shutdown of the upper and lower arms switches is called demagnetization state ($S = -1$).

For SRM, the torque ripple is caused by its unique double salient structure and discrete conduction mechanical characteristics, especially in the commutation region. In the DITC control strategy, the switching state of each phase is determined by the actual rotor position and torque error, and the torque error can be expressed as

$$\Delta T = T_{ref} - T_e \tag{1}$$

where ΔT is the torque error; T_{ref} is the reference torque; T_e is the electromagnetic torque.

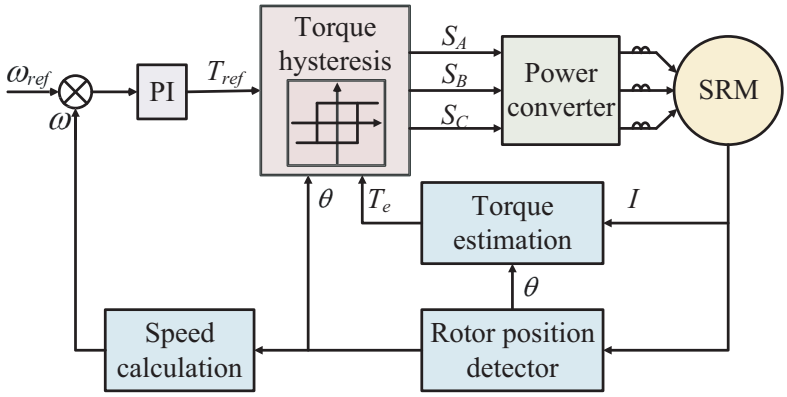

Figure 1. DITC system block diagram.

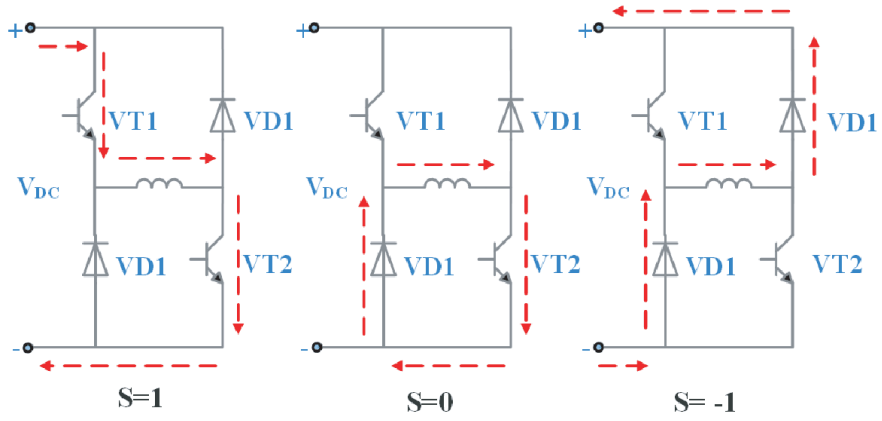

Figure 2. Asymmetric half bridge circuit.

According to the torque error, the traditional DITC formulates a set of hysteresis scheme. When the motor operating in single-phase, the switch tube only has excitation and freewheeling states, and the demagnetization state is not used to avoid excessive torque ripple. The hysteresis in single-phase region is shown in Fig. 3(a), where $T_{\min}$ and $T_{\max}$ are the minimum and maximum limits of torque error, respectively. During the commutation, the switching states of overlapping phases do not change at the same time. In order to ensure the smoothness of commutation, the control priority of outcoming and incoming phases should be considered properly. When $T_e > T_{ref}$, the outcoming phase acts as

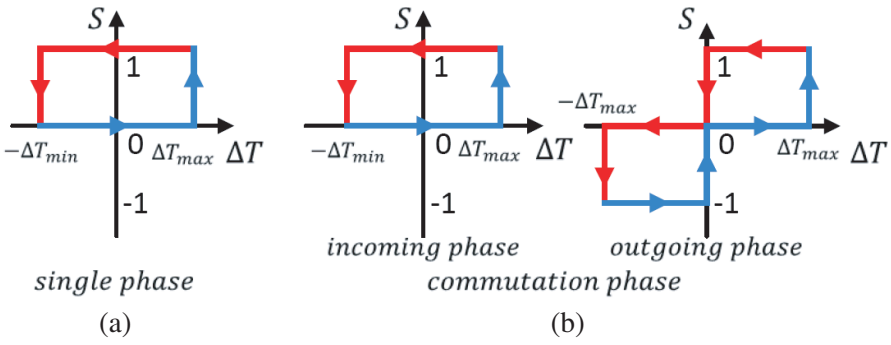

Figure 3. Traditional DITC hysteresis scheme. (a) Single-phase hysteresis. (b) Commutation-phase hysteresis.

demagnetizing phase to reduce the torque. When the generated torque is insufficient, the incoming phase will be the excitation phase which mainly generates torque, and the hysteresis in commutation region is shown in Fig. 3(b).

2.2. Analysis of Torque Ripple

Although the traditional DITC hysteresis scheme can effectively reduce the torque ripple, the suppression effect is not complete, and the torque ripple in commutation region is still too large. Due to the doubly salient structure of SRM, the torque is produced by the tendency of the rotor to move to its minimum reluctance position. In the case of ignoring the magnetic saturation effect, the torque is only determined by two variables: phase current and inductance slope. The change rate of SRM inductance with rotor position is the inherent property of the motor, and the stable electromagnetic torque can be obtained only by controlling the current and changing the inductance slope. The single-phase torque expression can be simply expressed as

$$T_k = \frac{1}{2} i_k^2 \frac{\mathrm{d}L_k}{\mathrm{d}\theta} \tag{2}$$

where T_k is the k-th phase torque; i_k is the k-th phase current; L_k is the k-th phase inductance; θ is the rotor position.

In the actual discrete control process, the change of the current is not with the smooth change of the theoretical curve, but with its serrated wave change in a certain range. So the torque waveform also is serrated, which is the cause of torque ripple.

As single-phase shown in Fig. 4(a), the regional inductance is approximately linear, and the slope of inductance with rotor position is very small. Therefore, according to formula (2), the corresponding torque slope is small. Before the torque monotonously increasing or decreasing to the hysteresis threshold, it needs to go through multiple sampling periods, as shown in the single-phase region of Fig. 4(b). At this time, the corresponding torque ripple is small.

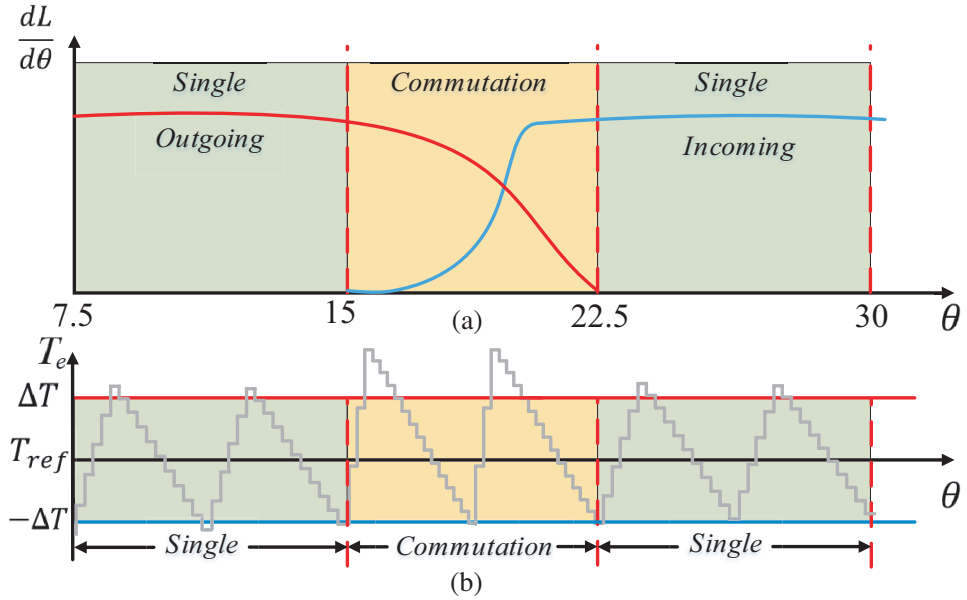

Figure 4. Torque analysis diagram. (a) Inductance angle slope diagram. (b) Torque hysteresis diagram.

In addition, the torque in commutation region is obtained by

$$T_{com} = \frac{1}{2} i_k^2 \frac{\mathrm{d}L_k}{\mathrm{d}\theta} + \frac{1}{2} i_{k+1}^2 \frac{\mathrm{d}L_{k+1}}{\mathrm{d}\theta} \tag{3}$$

where T_{com} is the sum of the two phases; i_{k+1} is the $k+1$-th phase current; L_{k+1} is the $k+1$-th phase inductance.

As shown in Fig. 4(a) commutation region, the torque is generated by the superposition of excitation phase and demagnetization phase, and the inductance regions of two phases are different. The excitation phase $\frac{dL}{d\theta}$ starts to rise from $\theta = 15°$, and the demagnetization phase decreases. The inductance slopes of the two phases are different and show nonlinear transformation, respectively. According to the principle of torque superposition, the slope of inductance increases. According to formula (3), the corresponding torque slope $\frac{dT}{dt}$ also increases, so the torque ripple in commutation region is larger, as shown in Fig. 4(b).

The torque generated by the minimum and maximum inductance regions of SRM under traditional DITC is not fully considered. Through the above analysis, when the SRM is single-phase operation, DITC can simply limit the torque ripple within the hysteresis range. However, after entering the commutation region, the excitation phase and demagnetization phase are in the critical state of minimum and maximum inductances, respectively. The torque slope in the commutation region is much higher than that in the single-phase region, so the hysteresis cannot effectively suppress the torque ripple in the commutation region.

Therefore, an advanced hysteresis optimal control strategy is very important to suppress the torque ripple of SRM. Taking into account the suppression of torque ripple within the effective hysteresis range and enhance the operating performance, an ADH-DITC strategy is proposed.

3. ADH-DITC OPTIMIZATION

3.1. Optimization Scheme of DITC Hysteresis Loop

Aiming at the causes of traditional DITC torque ripple, the hysteresis scheme is adjusted. When the motor works in single-phase, the torque slope is small, and the monotonous rise rate of torque is slow. It is not easy to exceed the limit of torque hysteresis, so the hysteresis scheme is retained, as shown in Fig. 5(a). When the motor is operating in the commutation region, the torque increases monotonously and rapidly, and only a few sampling times can exceed the hysteresis limit resulting in large torque ripple. The hysteresis adjustment scheme is shown in Fig. 5(b). i. As the phase is excitation phase, the phase is excited when the instantaneous torque T_{ins} is lower than the lower limit of hysteresis and enters freewheeling state when T_{ins} is higher than the upper limit of hysteresis. In order to establish the current, the phase is not demagnetized. ii. As the phase is demagnetized, the phase is freewheeled when T_{ins} is lower than the lower limit of hysteresis, and the phase enters the demagnelization state when the T_{ins} is higher than the upper limit of hysteresis. In order to reduce the rise rate of torque, the phase will not enter the excitation state.

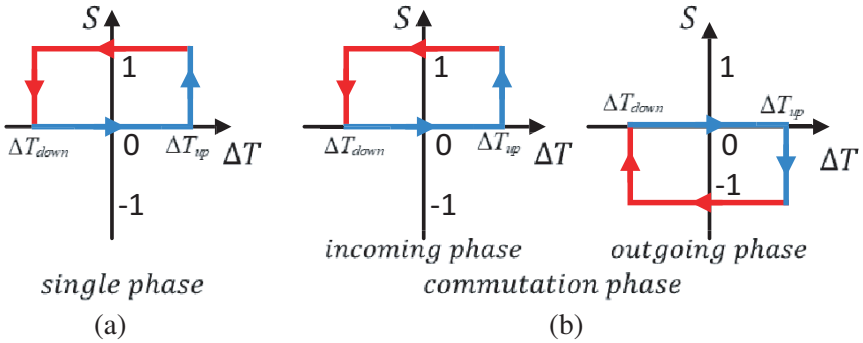

Figure 5. ADH-DITC hysteresis scheme. (a) Single-phase hysteresis. (b) Commutation-phase hysteresis.

When the torque increases in excitation phase, the corresponding demagnetization phase torque decreases. Because the two phases cancel each other, the torque slope after superposition will be reduced, and it is easier to adjust with ADH.

3.2. ADH-DITC

ADH is an online optimal control strategy based on torque slope. The torque slope at each rotor position is very important for the adaptive dynamic adjustment of hysteresis loop. The torque slope can be obtained by adding a sampling module, and the hysteresis threshold of the whole electrical cycle can be adjusted dynamically. According to the discrete property and hysteresis rule of SRM steady state operation, the torque change rate obtained by sampling is alternating positive and negative, so the complete data of torque growth rate or decline rate cannot be obtained. However, it can be seen from the existing data that the torque slope data are nonlinear, and the data densities in different intervals are different, as shown by the red line in Fig. 7(a). In this paper, the complete slope curve can be obtained by approximately compensating the non-sampled data, and ADH-DITC is proposed based on the torque slope curve.

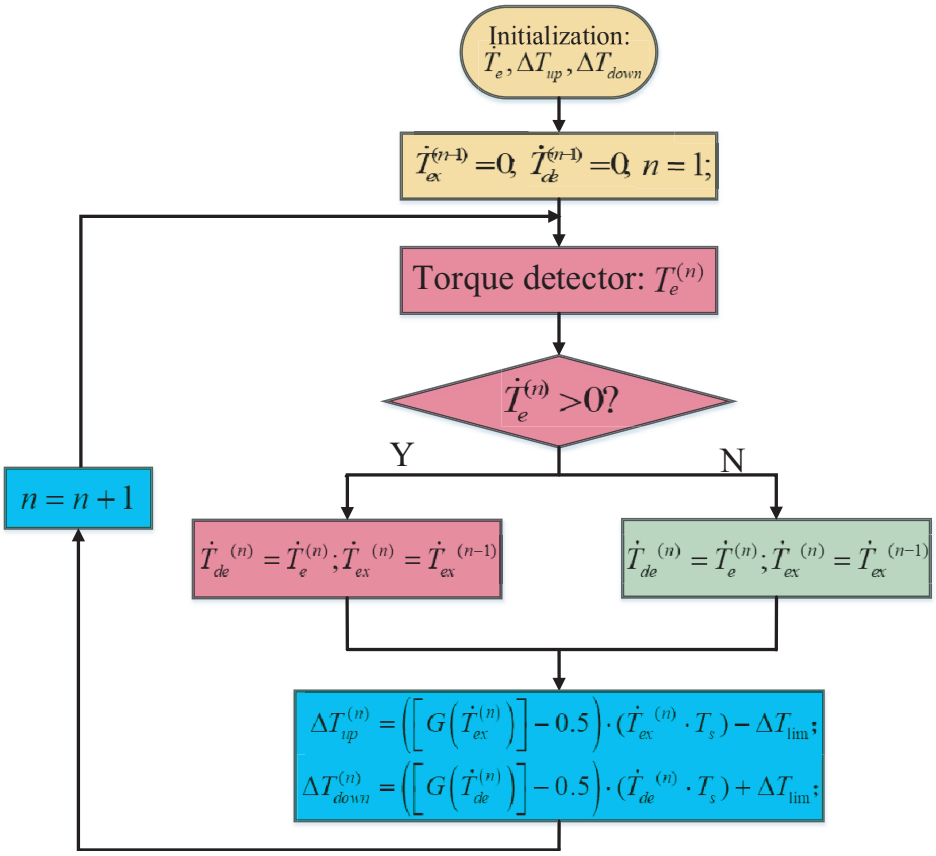

Figure 6. Flowchart of ADH generation.

The flowchart of ADH generation is shown in Fig. 6. Firstly, the torque slope $\dot{T}_e$ and dynamic hysteresis value $\Delta T_{up/down}$ are initialized. Secondly, in order to ensure the correctness of the system and the correct value of each torque slope, the values of excitation torque slope $\dot{T}_{ex}^{(n-1)}$ and demagnetization torque slope $\dot{T}_{de}^{(n-1)}$ should be set to zero first. Thirdly, the electromagnetic torque T_e of the motor is detected, and then the derivative value is judged for subsequent assignment operation.

If the value $\dot{T}_e^{(n)}$ after torque derivation is greater than zero, the moment is in the excitation state; only the slope data in the excitation state can be captured; the value is retained in the excitation torque slope; and the blank freewheeling torque slope is compensated by the previous value. Similarly, when the torque derivative value $\dot{T}_e^{(n)}$ is less than zero, the slope compensation method is the same under the

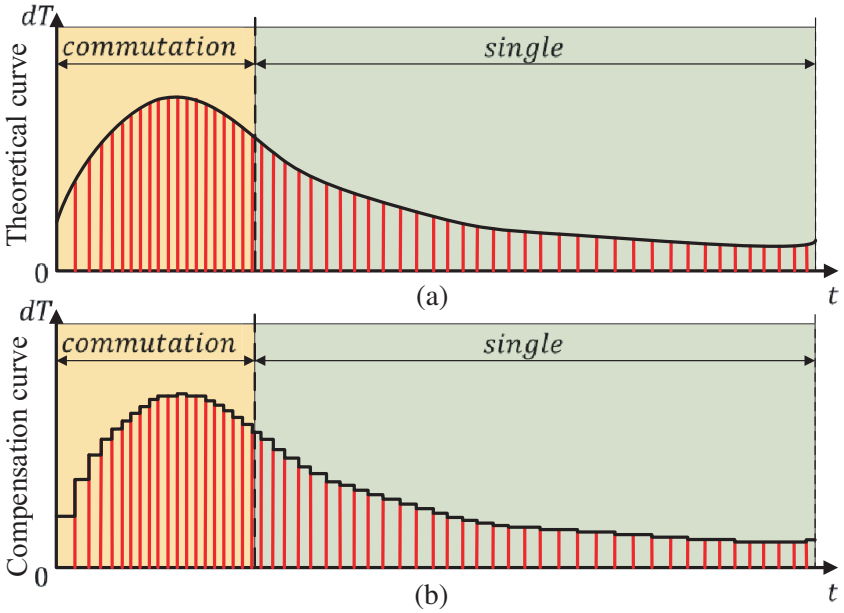

Figure 7. Torque slope curve. (a) Ideal curve. (b) Compensation curve.

motor freewheeling state. The calculation formulas are

$$\begin{cases} \dot{T}_{ex}^{(n)} = \dot{T}_{e}^{(n)} \\ \dot{T}_{de}^{(n)} = \dot{T}_{de}^{(n-1)} \end{cases}, \quad \dot{T}_{e}^{(n)} > 0 \tag{4}$$

$$\begin{cases} \dot{T}_{de}^{(n)} = \dot{T}_{e}^{(n)} \\ \dot{T}_{ex}^{(n)} = \dot{T}_{ex}^{(n-1)} \end{cases}, \quad \dot{T}_{e}^{(n)} < 0 \tag{5}$$

where n is the number of samples; $\dot{T}_{ex}$ is the slope of excitation torque; $\dot{T}_{de}$ is the slope of demagnetization torque; $\dot{T}_e$ is the torque slope.

According to the above compensation principle, the complete torque slope curve in one cycle is shown in Fig. 7(b). Since the data density in commutation section is much higher than that in single-phase section, the compensation accuracy in commutation section is higher. Compared with the theoretical slope curve in Fig. 7(a), the compensation accuracy in Fig. 7(b) can meet the estimation requirements of adaptive dynamic hysteresis, and the system can be adjusted adaptively in real time, with small amount of calculation and without increasing the complexity of the system.

Finally, the dynamic hysteresis is obtained by the following formula

$$G(x) = \left| \frac{\Delta T}{T_s \cdot x} \right| \tag{6}$$

$$\Delta T_{up}^{(n)} = \left(\left[G\left(\dot{T}_{ex}^{(n)} \right) \right] - 0.5 \right) \cdot \left(\dot{T}_{ex}^{(n)} \cdot T_s \right) - \Delta T_{\lim} \tag{7}$$

$$\Delta T_{down}^{(n)} = \left(\left[G\left(\dot{T}_{de}^{(n)} \right) \right] - 0.5 \right) \cdot \left(\dot{T}_{de}^{(n)} \cdot T_s \right) + \Delta T_{\lim} \tag{8}$$

where G is the growth factor; ΔT_{up} is the upper limit of dynamic hysteresis; ΔT_{down} is the lower limit of dynamic hysteresis; ΔT_{lim} is the maximum allowable limit of hysteresis.

In an excitation process, according to formula (7), the value of ΔT_{up} is determined by the growth factor G when the torque monotonically rises to the upper limit. Because the torque slope curve is nonlinear, the calculation result of G is not an integer, rounding it and subtracting 0.5 to ensure the effective triggering of the hysteresis controller. Multiplying G and $\dot{T}_{ex}$, then subtracting ΔT_{lim} to get the upper limit of dynamic hysteresis ΔT_{up}, the same applies to the lower limit ΔT_{down}. The dynamic hysteresis can act on the whole operation cycle, and the hysteresis threshold can be adjusted in real time

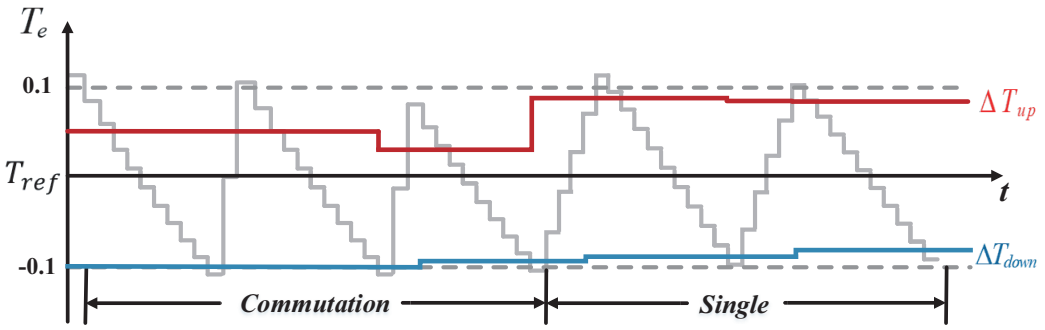

Figure 8. The dynamic hysteresis diagram.

with the corresponding torque slope under different rotor positions, so as to ensure that the torque ripple is limited within the upper and lower limits of the hysteresis at each excitation or demagnetization. The dynamic hysteresis diagram is shown in Fig. 8.

4. SIMULATION VERIFICATION

The ADH simulation model in this paper is built in MATLAB/Simulink module. The phase current and instantaneous electromagnetic torque in the simulation are obtained by look-up table. The parameters of the corresponding SRM prototype are shown in Table 1, and the prototype of the SRM is shown in Fig. 9. In order to verify the improvement of commutation smoothness and torque suppression effect of the proposed control method, the traditional control schemes CCC, DITC, and the proposed control scheme ADH-DITC are analyzed and compared. The simulation results are as follows.

Table 1. Parameters of the SRM.

Motor parameters	value	Motor parameters	value
Stator/rotor poles	12/8	Rated speed(r/min)	1500
Power (kW)	2.2	Stator resistance (Ω)	0.6
Rated torque ($N \cdot m$)	14	Moment of inertia ($kg \cdot m^2$)	0.01

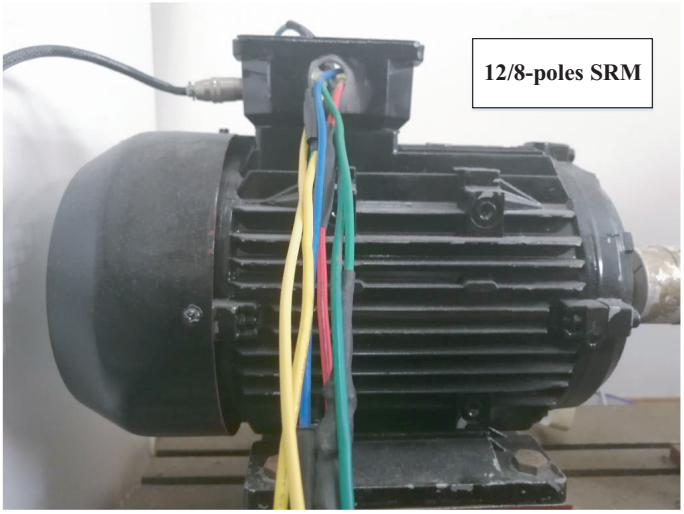

Figure 9. 12/8-poles SRM.

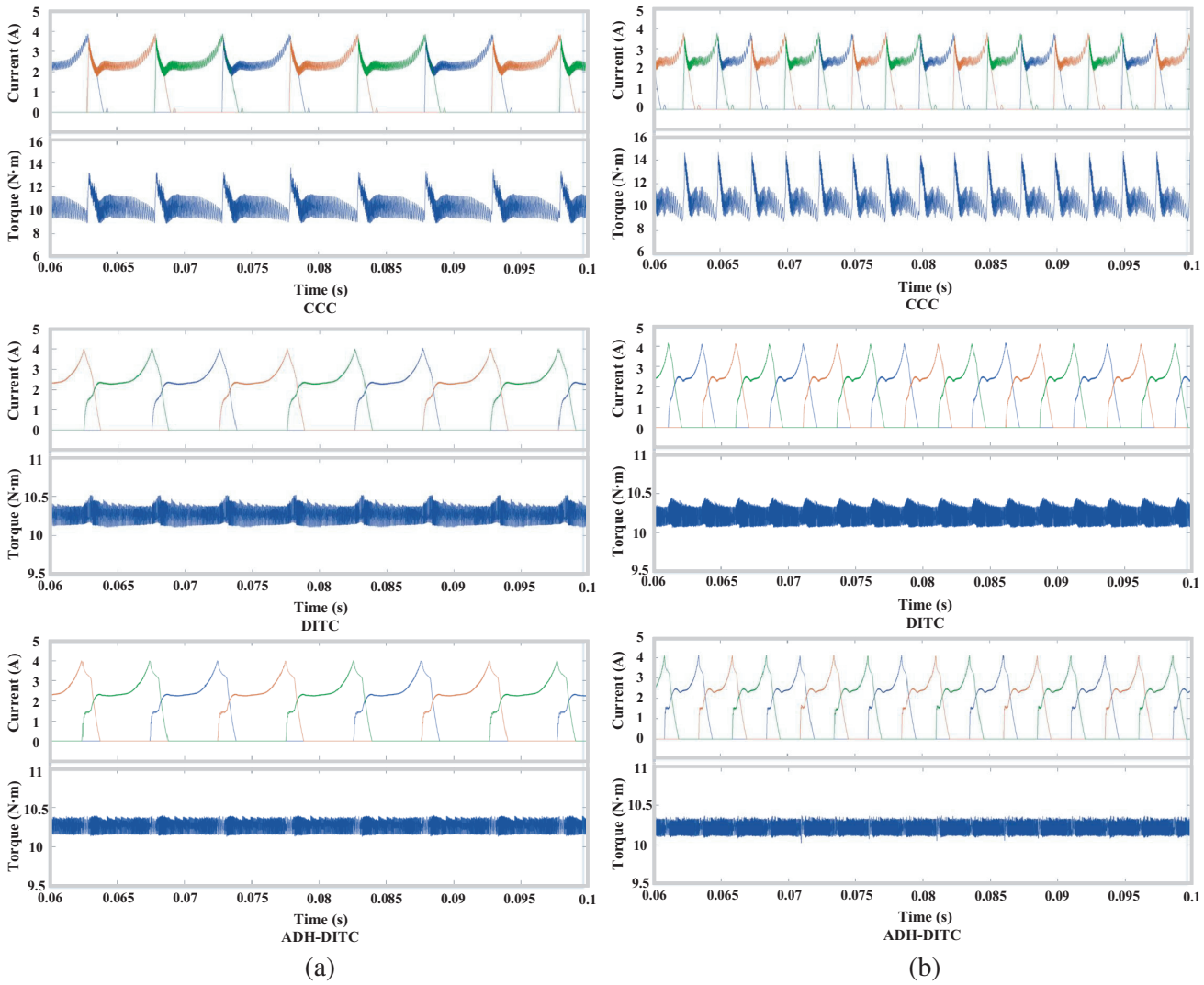

Figure 10. Phase current and total torque at 10 N · m. (a) 500 rpm. (b) 1000 rpm.

Figure 10 shows the torque and phase current results of three control schemes at different speeds when the load torque is 10 N · m, where Fig. 10(a) is 500 rpm, and Fig. 10(b) is 1000 rpm. The phase current hysteresis width of CCC is 0.5 A; the outer and inner torque hysteresis widths of traditional DITC are 0.12 N · m and 0.1 N · m, respectively; and the maximum torque hysteresis value of ADH-DITC is 0.1 N · m. The actual hysteresis value is dynamic. Fig. 11 shows a section of ADH at 1000 rpm.

In order to intuitively reflect the optimal performance of the proposed ADH scheme, the standard deviation T_{std} and torque ripple coefficient T_r are introduced as the system evaluation indexes. When SRM is operating in steady state under CCC, DITC, and ADH-DITC, respectively, sampling the T_e in one cycle, then substituting the sampled data into formula (9) to obtain T_{std} and T_r, the formula is as follows

$$T_{std} = \sqrt{\frac{\sum_{j=1}^{m} (T_e - T_{av})^2}{m}}, \quad T_r = \frac{T_{\max} - T_{\min}}{T_{avg}} \tag{9}$$

where m is the number of samples; T_e is the electromagnetic torque of the j sampling point; T_{avg} is the average value of sampling torque; $T_{\max}$ and $T_{\min}$ are the maximum and minimum of torque ripple, respectively.

Table 2. Comparison results of torque standard deviation and torque ripple coefficient.

Speed	Method	Torque standard deviation	Torque ripple coefficient
500 rpm	CCC	76.84%	40.36%
	Traditional method	8.11%	3.42%
	Proposed method	6.17%	2.52%
1000 rpm	CCC	76.72%	47.09%
	Traditional method	8.05%	3.97%
	Proposed method	6.13%	2.56%

Table 2 shows the torque standard deviation and torque ripple coefficient of CCC, DITC, and ADH-DITC at different speeds of 10 N · m.

As shown in Fig. 10, compared with the traditional CCC and DITC, the proposed method has better effect on improving the smooth performance of the motor in steady state. Fig. 11 shows that the hysteresis value of ADH-DITC changes in real time, confirming the correctness of the theoretical derivation. Table 2 shows that the proposed algorithm has better torque ripple suppression effect and fully limits the torque ripple within the maximum allowable hysteresis range.

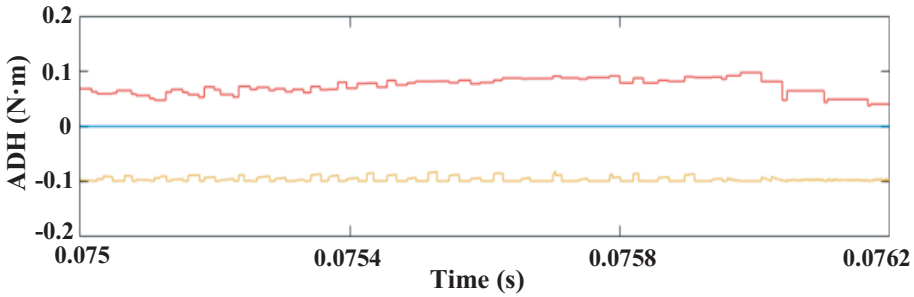

Figure 11. A section of ADH at 1000 rpm.

Figure 12 shows the torque mutation waveforms of the two methods when the load torque is from 8 N · m to 12 N · m at 1000 rpm. It can be seen from the figure that both methods have good dynamic response, but the torque amplitude of the proposed optimization method is smaller than that of the traditional DITC. It also shows that ADH can optimize DITC in real time.

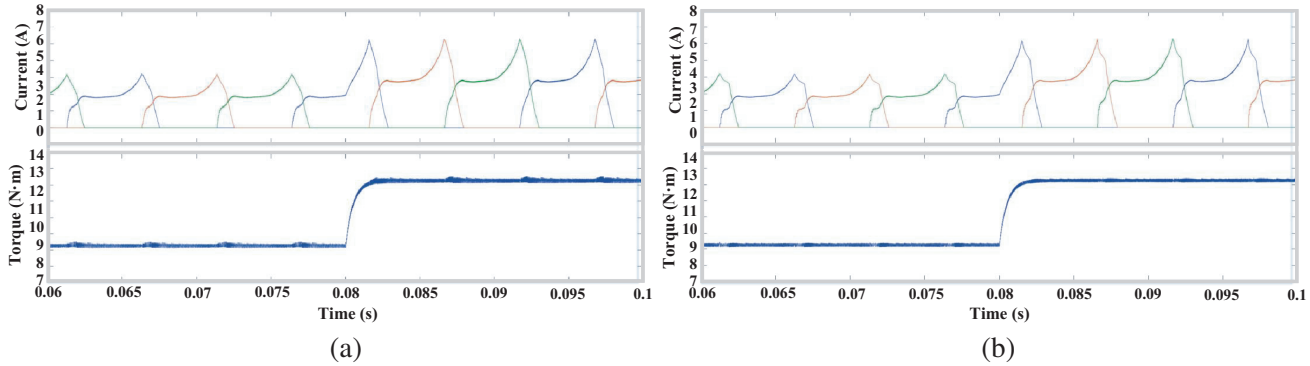

Figure 12. Dynamic waveform of torque. (a) DITC. (b) ADH-DITC.

5. CONCLUSION

Based on the torque slope characteristics of SRM, an ADH control scheme with optimized DITC is proposed in this paper. By analyzing the torque characteristics and hysteresis rules of SRM in different conductive regions, the torque slope is taken as the adjustment standard of ADH. Firstly, the traditional hysteresis control scheme is modified. Secondly, the sampled discrete torque slope data are compensated online. Finally, the hysteresis threshold is calculated in real time according to the compensation results, so as to achieve the purpose of ADH adjustment for each rotor position. Detailed simulation results show that this method can improve the efficiency and torque tracking accuracy of SRM, and effectively reduce the torque ripple without additional complexity.

REFERENCES

1. Zhu, Y., C. Zhao, J. Zhang, and Z. Gong, "Vibration control for electric vehicles with in-wheel switched reluctance motor drive system," *IEEE Access*, Vol. 8, 7205–7216, 2020.
2. Ho, C., J. Wang, K. Hu, and C. Liaw, "Development and operation control of a switched-reluctance motor driven flywheel," *in IEEE Transactions on Power Electronics*, Vol. 34, No. 1, 526–537, 2019.
3. Li, S., S. Zhang, T. G. Habetler, and R. G. Harley, "Modeling, design optimization, and applications of switched reluctance machines — A review," *IEEE Transactions on Industry Applications*, Vol. 55, No. 3, 2660–2681, 2019.
4. Mousavi-Aghdam, S. R., M. R. Feyzi, N. Bianchi, and M. Morandin, "Design and analysis of a novel high-torque stator-segmented SRM," *IEEE Transactions on Industrial Electronics*, Vol. 63, No. 3, 1458–1466, 2016.
5. Hu, Y., W. Ding, T. Wang, et al., "Investigation on a multimode switched reluctance motor: Design, optimization, electromagnetic analysis, and experiment," *IEEE Transactions on Industrial Electronics*, Vol. 64, No. 12, 9886–9895, 2017.
6. Xu, Z., M.-J. Kim, D. Lee, and J. Ahn, "Characteristics analysis and comparison of conventional and segmental rotor type 12/8 switched reluctance motors," *2016 IEEE Industry Applications Society Annual Meeting*, 1–7, 2016.
7. Mikail, R., I. Husain, Y. Sozer, et al., "A fixed switching frequency predictive current control method for switched reluctance machines," *2012 IEEE Energy Conversion Congress and Exposition (ECCE)*, 843–847, 2012.
8. Mikail, R., I. Husain, M. S. Islam, Y. Sozer, et al., "Four-quadrant torque ripple minimization of switched reluctance machine through current profiling with mitigation of rotor eccentricity problem and sensor errors," *IEEE Transactions on Industry Applications*, Vol. 51, No. 3, 2097–2104, 2015.
9. Dowlatshahi, M., S. M. Saghaian-Nejad, M. Afshoon, et al., "High efficient torque control of switched reluctance motor taking nonlinear and saturation effects into account," *4th Annual International Power Electronics*, 49–54, 2013.
10. Lee, D., J. Liang, Z. Lee, et al., "A simple nonlinear logical torque sharing function for low-torque ripple SR drive," *IEEE Transactions on Industry Applications*, Vol. 56, No. 8, 3021–3028, 2009.
11. Mitra, R., W. Uddin, Y. Sozer, et al., "Torque ripple minimization of Switched Reluctance Motors using speed signal based phase current profiling," *2013 IEEE Energytech*, 1–5, 2013.
12. Xu, A., C. Shang, J. Chen, J. Zhu, and L. Han, "A new control method based on DTC and MPC to reduce torque ripple in SRM," *IEEE Access*, Vol. 7, 68584–68593, 2019.
13. Xu, A., W. Zhang, L. Han, et al., "Minimising torque ripple of switched reluctance motor by applying deadbeat-direct torque and flux control," *IET Electric Power Applications*, Vol. 13, No. 11, 1883–1890, 2019.
14. Pittam, K. R., D. Ronanki, and P. Parthiban, "Efficiency improvement of four-phase switched reluctance motor drive using new direct torque control strategy," *IET Electric Power Applications*, Vol. 14, No. 1, 52–61, 2020.

15. Yan, N., X. Cao, and Z. Deng, "Direct torque control for switched reluctance motor to obtain high Torque-Ampere ratio," *IEEE Transactions on Industrial Electronics*, Vol. 66, No. 7, 5144–5152, 2019.
16. Weiss, C. P., S. Schoeler, and R. Doncker, "Direct instantaneous torque control for switched reluctance machines considering mutual coupling," *The Journal of Engineering*, Vol. 17, 3701–3704, 2019.
17. Gan, C., Q. Sun, Y. Hu, et al., "Low-cost direct instantaneous torque control for switched reluctance motors with bus current detection under soft-chopping mode," *IET Power Electronics*, Vol. 9, No. 3, 482–490, 2016.
18. Wang, S., Z. Hu, and X. Cui, "Research on novel direct instantaneous torque control strategy for switched reluctance motor," *IEEE Access*, Vol. 8, 66910–66916, 2020.
19. Song, S., G. Fang, R. Hei, J. Jiang, et al., "Torque ripple and efficiency online optimization of switched reluctance machine based on torque per ampere characteristics," *IEEE Transactions on Power Electronics*, Vol. 35, No. 9, 9608–9616, 2020.
20. Sun, Q., J. Wu, and C. Gan, "Optimized direct instantaneous torque control for SRMs with efficiency improvement," *IEEE Transactions on Industrial Electronics*, Vol. 68, No. 3, 2072–2082, 2021.